A comprehensive study on active Lamb wave-based damage identification for plate-type structures

Zijian Wang[*1], Pizhong Qiao[2a] and Binkai Shi[3b]

[1]*Department of Dam Safety Management, Nanjing Hydraulic Research Institute, Nanjing, 210029, China*
[2]*Department of Civil and Environmental Engineering and Composite Materials and Engineering Center,*
Washington State University, Pullman, WA, 99164-2910, USA
[3]*School of Mechanics and Materials, Hohai University, Nanjing, 210098, PR China*

Abstract.   Wear and aging associated damage is a severe problem for safety and maintenance of engineering structures. To acquire structural operational state and provide warning about different types of damage, research on damage identification has gained increasing popularity in recent years. Among various damage identification methods, the Lamb wave-based methods have shown promising suitability and potential for damage identification of plate-type structures. In this paper, a comprehensive study was presented to elaborate four remarkable aspects regarding the Lamb wave-based damage identification method for plate-type structures, including wave velocity, signal denoising, image reconstruction, and sensor layout. Conclusions and path forward were summarized and classified serving as a starting point for research and application in this area.

Keywords: Lamb wave; damage identification; structural health monitoring; wavelet denoising; finite element modeling; sensor array; beamforming

1. Introduction

Engineering structures sustain strength degradation due to wear, aging, corrosion, overload, fatigue, and unexpected scenarios throughout their service life. It is economical and risk-free to examine their state in real time and conduct predictive maintenance (Fan and Qiao 2011). Therefore, increasing attentions have been devoted to the structural health monitoring (SHM), which primarily includes five stages (Farrar and Worden 2007): 1) data acquisition, cleansing and storage; 2) damage identification and pattern recognition; 3) information condensation and statistical model development; 4) remaining life prognosis; and 5) damage control and self-healing. As a crucial part of the SHM, damage identification aims to prevent catastrophic failure and improve structural reliability. Among various methods, Lamb waves are a promising technique suitable for damage identification of plate-type structures (Mitra and Gopalakrishnan 2016). Comparing with bulk waves, which can be seen as the waves traveling in infinite media, Lamb waves can irradiate over structural thickness and propagate long distance with consistent waveforms, providing rapid assessments over substantial areas. Since damage changes structural acoustic property and causes wave scattering,

damage can be identified according to change of Lamb wave parameter (e.g., phase, maximum amplitude, rise time, duration, energy, and correlation coefficients). The occurrence and location of damage can be identified based on the time interval between incident and scattered waves (Chen *et al.* 2016); while the severity of damage can be evaluated based on the amplitude of reflected (Yang *et al.* 2017) and/or transmitted waves (Yang and Ume 2017).

During the process of Lamb wave-based damage identification, attention should be paid to four aspects to secure reliable and accurate results. First, the wave velocity changes with tuning frequency (Zhu *et al.* 2017), vibration mode (Yang *et al.* 2016), and propagation direction (Ratassepp *et al.* 2016). Therefore, accurate damage identification requires effective compensation of wave dispersion (Cai *et al.* 2017), feasible separation of vibration modes (Ambrozinski and Stepinski 2017), and proper consideration of directional velocity (Sause *et al.* 2013). Second, when Lamb waves travel in high-damping medium at long distance with limited excitation power, environmental noises merge into monitoring signals. Therefore, signal denoising is desirable to interpret monitoring signal and differentiate the wave peaks of interest (De Marchi *et al.* 2017). Third, since monitoring signals received by sensors are one dimensional, it is imperative to convert them to a two dimensional image to quantitatively present location, shape and severity of damage (Muller *et al.* 2017). To this end, a variety of image reconstruction algorithms with their own strength and weakness have been developed (Aryan *et al.* 2017, Wang and Qiao 2017, Zeng *et al.* 2017). Since image reconstruction algorithms can influence damage representation, the discussion on this aspect is of necessity.

∗Corresponding author, Ph.D.
  E-mail: zijianwang@nhri.cn
[a] Professor
  E-mail: Qiao@wsu.edu
[b] Ph.D. Student
  E-mail: hhusbk2009@hhu.edu.cn

Finally, the layout of sensor array can influence the superposition of wave excited by each transmitter and thus influence energy focused in a given direction (Yu and Giurgiutiu 2008). To improve the directivity of sensor array, it is necessary to optimize sensor layout, so that sensor array can generate concentrated beam to identify tiny damage.

In this paper, a comprehensive study was conducted to elaborate four aspects associated with the Lamb wave-based damage identification of plate-type structures by finite element simulations. In the end, basic techniques and points as well as remarkable conclusions and path forward were summarized and classified, serving as a starting point for research and application in this area.

2. Wave velocity

Accurate calculation of the distance between damage and sensor depends on precise knowledge of wave velocity. To characterize dispersive Lamb wave velocities caused by anisotropic media and boundary constraints, dispersion and wavefront curves are developed.

The dispersion curve characterizes the variation of wave velocity according to tuning frequency, as well as the presence of multiple vibration modes. For single-layered medium, the propagation of Lamb wave follows the Navier equation (Su *et al.* 2006)

$$\mu\nabla^2 u + (\lambda + \mu)\nabla(\nabla \cdot u) = \rho\frac{\partial^2 u}{\partial t^2} \qquad (1)$$

where u is the displacement vector; ρ is the density; λ and μ are the Lamé constants. By introducing boundary conditions at surfaces, the dispersion curve can be plotted as eigenvalues of the characteristic equation. For multi-layered medium, the matrix-based methods, e.g., the transfer (Wang and Yuan 2007) and global (Pant *et al.* 2014) matrix method, are developed to consider the continuity at interfaces. The basic procedure of these matrix-based methods is to solve the displacement and stress in each layer and assemble these physical quantities to form the characteristic equation.

For instance, an AL6061-T6 aluminum plate was selected to produce the dispersion curve of single-layered medium, while fiber reinforced epoxy laminated composite of $[0/90]_{2s}$ sequence was selected to produce the dispersion curve of multi-layered medium. The material properties of aluminum and fiber reinforced epoxy laminated composite are shown in Tables 1 and 2, respectively. These dispersion curves indicate that the Lamb wave velocity is dependent with the product of tuning frequency and plate thickness, as shown in Fig. 1. According to the displacement about mid-plane, Lamb waves can be classified as symmetric (denoted by S) and anti-symmetric (denoted by A) mode. With the rise of tuning frequency, multiple vibration modes are presented in the dispersion curves.

Another approach to characterize Lamb wave velocity is the wavefront curve. For the Lamb wave propagation in anisotropic medium, wave velocity varies with the propagation direction. The wavefront curve shows the locus of admitted wave velocity in all directions for a given

frequency, as shown in Fig. 2. For the fiber reinforced epoxy laminate of $[0/90]_{2s}$ sequence, Lamb waves propagate faster along 0° and 90° due to the fiber reinforcement in these directions, resulting in directional wave velocity under the excitation of 100 kHz. To identify damage in anisotropic medium, the wave velocity should be appropriately calculated according to different wave paths.

Meanwhile, various spectral methods have been developed to measure the wave velocities in field and experiment. The phase velocity can be determined according to the phase delays between different locations along the wave path through the Slant-Stack transformation (Ambrozinski *et al.* 2014); while the group velocity can be determined according to the energy distribution in time and frequency domains through the short-time Fourier transformation (Niethammer *et al.* 2000).

(a) Single-layered medium
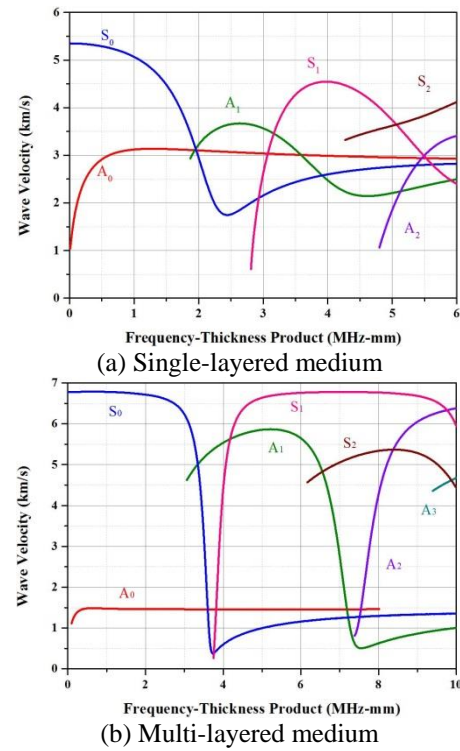

(b) Multi-layered medium
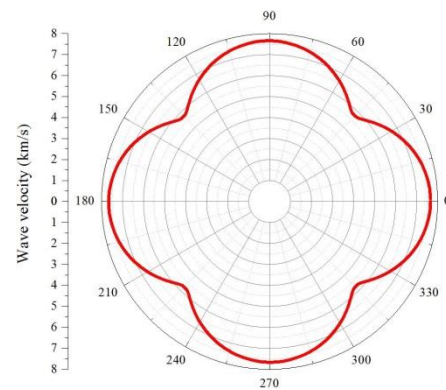
Fig. 1 The dispersion curves of Lamb waves

Fig. 2 The wavefront curve of fiber reinforced epoxy laminated composite

Table 1 Material properties of aluminum

Young's modulus E (GPa)	Poisson ratio v	Density ρ (g/cm^3)
68.9	0.33	2.7

Table 2 Equivalent material properties of fiber reinforced epoxy laminated composite

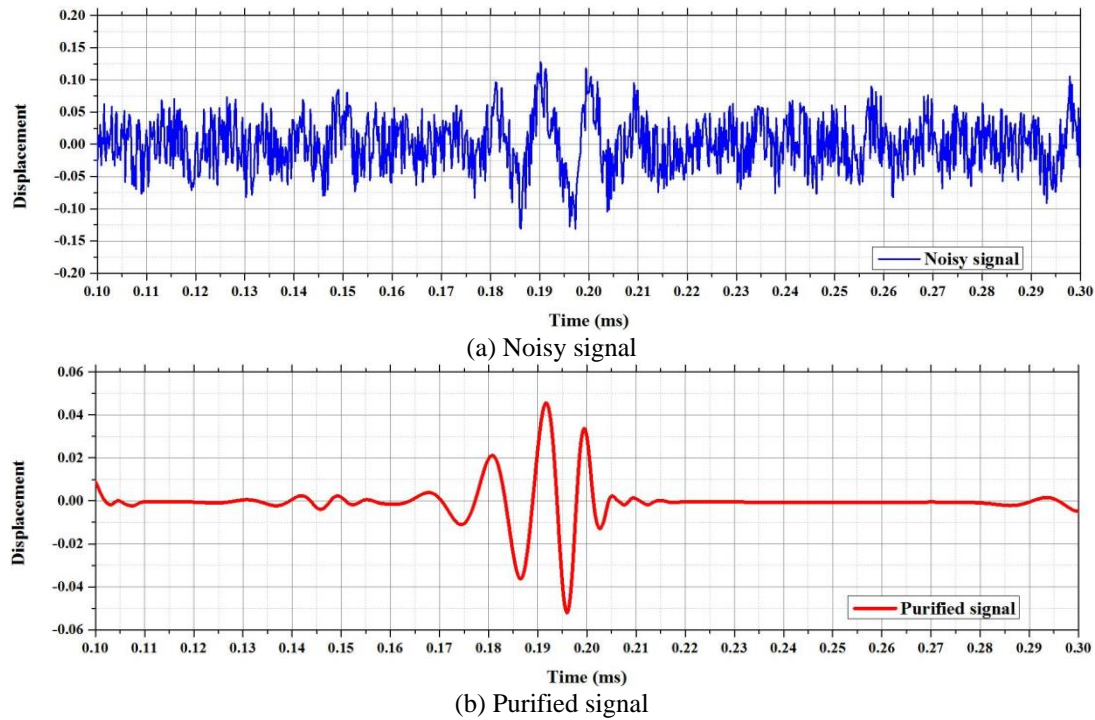| E_1 (GPa)	E_2 (GPa)	G_{12} (GPa)	G_{13} (GPa)	v_{12}	v_{13}	v_{23}	ρ (g/cm^3)
175.9	8.73	4.49	4.49	0.34	0.34	0.28	1.576

(a) Noisy signal

(b) Purified signal

Fig. 3 Signals before and after wavelet denoising

3. Signal denoising

The frequency of Lamb waves used in damage identification is normally from 10 kHz to 1 MHz, which overlaps with the frequency of electromagnetic waves (Verona *et al.* 2017). When Lamb wave-based damage identification is performed in electromagnetic interferences, the signal to noise ratio decreases (Wang *et al.* 2016). Another reason causing the decrease of signal to noise ratio of monitoring signals is the attenuation of Lamb waves. The attenuation is related to the propagation distance, property of medium (Tao *et al.* 2017), vibration mode (Bonnel *et al.* 2017), frequency (Zeng *et al.* 2017), and excitation parameter (Birgani *et al.* 2017). To extend the use of Lamb wave-based damage identification to realistic scenarios, signal denoising has been adopted to purify monitoring signals and make damage-related wave features more distinctively. The wavelet denoising has been demonstrated as an effective method for Lamb wave signal denoising (Kabir and Shahnaz 2012). The damage-related waves with limited frequency band appear in some certain components of the wavelet decomposition, while interferences appear in the others. By depressing the component out of interest, purified signal can be synthesized through the inverse wavelet transform.

As an example to demonstrate signal denoising, a process of corrosion identification was simulated on an aluminum shell. The cylindrical aluminum shell with dimensions of 1 m × 1 m × 1 mm was modeled by extruding a curvy line with a curvature of 0.8 in Abaqus explicit. Considering accuracy and efficiency, the element was set to *S4R* in 1 × 1 mm, and the time increment was set to 1 × 10^{-7} s. Four sensors were at the location of (200, 200), (-200, 200), (-200, -200) and (200, -200) mm according to the Cartesian coordinate at shell center. The corrosion was simulated in a 30 × 30 mm rectangular region whose stiffness was reduced by 50%. The left bottom corner of the corrosion region was at the location of (100, 0) mm. A 5-cycle sinusoid tone burst (100 kHz) was applied as a nodal displacement out of the plate to excite Lamb waves. By exciting four sensors in turns, 12 monitoring signals were recorded. To make the scenario more realistic, 50%

Gaussian noises were artificially mixed to the monitoring signals.

The damage reflections were extracted by subtracting baselines from monitoring signals. Due to the comparable amplitude of Gaussian noises, damage reflection cannot be distinguished from time domain directly, as shown in Fig. 3(a). Then, the wavelet decomposition was performed to obtain a series of details and approximations. Since the Gaussian noises exist in high-level details, the wavelet denoising aims to depress the strength of these high-level details. By setting the coefficients $\hat{d}_j$ to some fraction of detail d_j, a threshold is thus applied on each detail to restrict their amplitude.

$$\hat{d}_j = \begin{cases} \text{sgn}(d_j)(|d_j| - e), & |d_j| \geq e \\ 0, & |d_j| < e \end{cases} \quad (2)$$

The threshold e is as follows

$$e = \sigma\sqrt{2\ln N} \quad (3)$$

$$\sigma = \frac{median(|d_1|)}{0.6745} \quad (4)$$

where d_1 is the 1st detail, and N is the number of sampling points. Then, the purified signals were reconstructed through the original approximation and depressed details. Through this process, the damage reflection is clearly presented at 0.2 ms, as shown in Fig. 3(b).
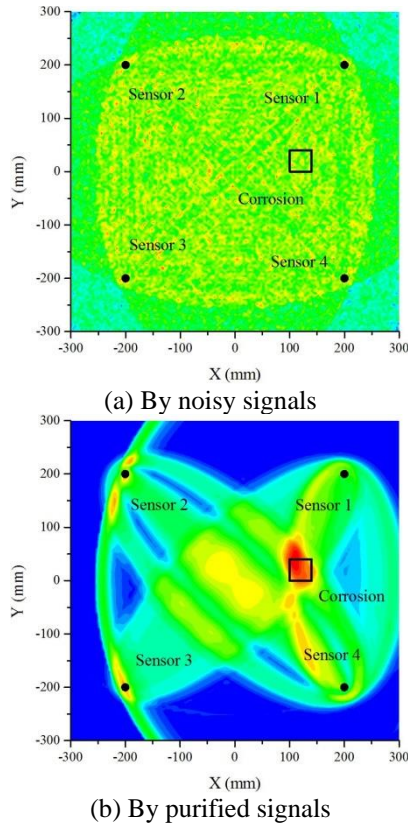

(a) By noisy signals

(b) By purified signals

Fig. 4 Reconstructed damage image showing corrosion identification

Furthermore, damage images generated by noisy and purified signals are plotted in Figs. 4(a) and 4(b), respectively. Since noises merge into the damage reflection, the reconstructed image is compromised, presenting no conclusive damage identification in Fig. 4(a). In contrast, the damage image generated by purified signals robustly identifies the corrosion with large pixels (red region), which accords with the actual location of corrosion (black rectangle), as shown in Fig. 4(b).

4. Image reconstruction

Since monitoring signals are one dimensional, it is imperative to convert them to a two dimensional damage image capable of quantitatively characterizing the degree of damage at each location over the structure. To this end, a variety of image reconstruction algorithms with their own strength and weakness have been developed (Wang *et al.* 2004, Cai *et al.* 2011, Zhang *et al.* 2017). Theses algorithms investigate the amplitude of differential signal (the difference between monitoring signal and baseline) to find abnormalities. By multiplying the time interval between excitation and reception with the wave velocity, the amplitude of differential signal can be used as a pixel value at each location over the structure. At this point, the superposition of pixels determined by different sensor pairs can produce a damage image showing the location, size and shape of identified damage.

In this section, two popular image reconstruction algorithms, i.e., delay and sum (DAS) algorithm and reconstruction algorithm for probabilistic inspection of defects (RAPID), were compared based on the same monitoring signals. The pixel in DAS algorithm (Malinowski *et al.* 2011) is defined as follows

$$P_{xy} = \int_{t_1}^{t_2} \vec{h}_{xy}(t)\vec{h}_{xy}^H(t)dt \quad (5)$$

$$\vec{h}_{xy}^M(t) = \left| \hat{h}_{xy}^M(t + \frac{d_{xy}^M}{c_g}) \right| \quad (6)$$

where $\vec{h}_{xy}^M$ is the envelope for *M*-th sensor pair produced by Hilbert transform; d_{xy}^M is the distance of wave path; and superscript *H* denotes the conjugate transpose. On the other hand, the pixel in RAPID (Yan *et al.* 2010) of the *ij*-th sensor pair (*i*-th sensor excites and *j*-th sensor receives) is defined as follows

$$P(x, y) = \sum_{i=1}^{N-1} \sum_{j=i+1}^{N} SDC_{ij} s_{ij} \quad (7)$$

The SDC_{ij} is the coefficients representing the correlating degree between monitoring signal S and baseline $\bar{S}$

$$SDC_{ij} = 1 - \left| \frac{\int (S_i(t) - \bar{S}_i)(S_j(t) - \bar{S}_j)dt}{\sqrt{\int (S_i(t) - \bar{S}_i)^2 dt \int (S_j(t) - \bar{S}_j)^2 dt}} \right| \quad (8)$$

And s_{ij} is defined as follows

$$s_{ij} = \frac{\beta - R_{ij}(x, y)}{\beta - 1} \quad \text{when} \quad \beta > R_{ij}(x, y) \tag{9}$$

$$R_{ij}(x, y) = \frac{\sqrt{(x-x_i)^2 + (y-y_i)^2} + \sqrt{(x-x_j)^2 + (y-y_j)^2}}{\sqrt{(x_i-x_j)^2 + (y_i-y_j)^2}} \tag{10}$$

where β is the scaling parameter around 1.05.

Then, the monitoring signals were extracted from finite element model and imported to the DAS and RAPID algorithms to reconstruct damage images, respectively.

The process of damage identification was simulated in a 1 m × 1 m × 1 mm aluminum plate which was discretized by *S4R* element (1 × 1 mm). The time increment was set to 1×10^{-6} s, and the excitation was set to 3.5-cycle Hanning windowed sinusoids (100 kHz). Sensors were placed around the plate in a circle of 400 mm radius to monitor surrounded area. Two holes with radius of 20 mm were drilled through thickness at the location of (0, 350) and (142, 142) mm, respectively, according to the Cartesian coordinate located at plate center. The sensors were excited in turns on healthy and damaged plates to collect baseline and monitoring signals separately.

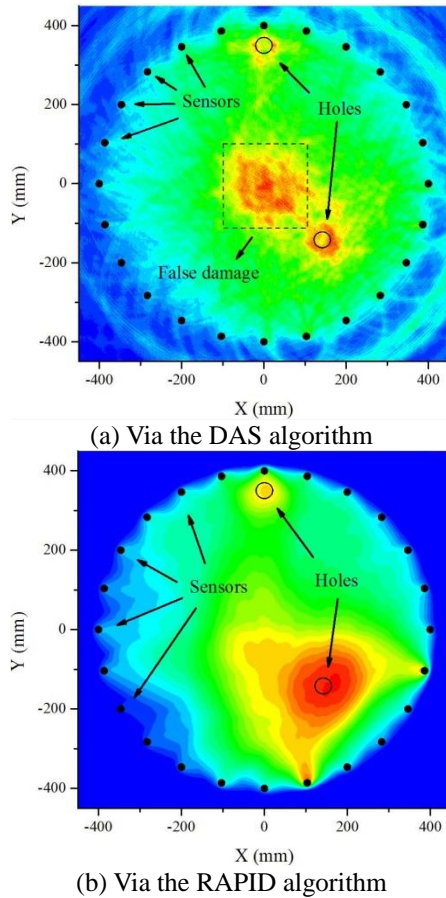(a) Via the DAS algorithm

(b) Via the RAPID algorithm

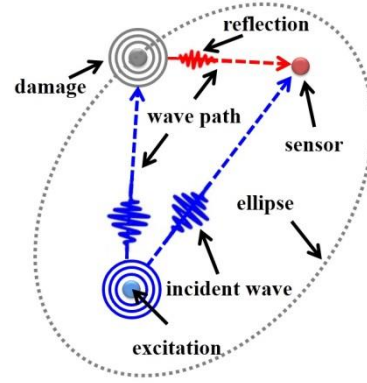Fig. 5 Reconstructed damage images

Fig. 6 Ellipse determined by single sensor pair

Damage images reconstructed by the DAS and RAPID algorithms are shown in Figs. 5(a) and 5(b), respectively. The DAS one has higher local resolution with more concentrated red pixels at actual damage locations; whereas the RAPID shows diffused damage identification. Besides, the DAS shows accurate identification roughly with the same shape as a circle (high pixels are concentrated around the actual hole edge); whereas the RAPID shows blurry identification of damage shape (high pixels form a thick peak covering the hole center). However, in the DAS algorithm, wave peaks in each differential signal assign high pixels in an ellipse pattern (see Fig. 6). These ellipses determined by different sensor pairs lead to superposition at the plate center, which could be falsely identified as damages, as shown in Fig. 5(a). In contrast, the RAPID based on the probability of damage occurrence robustly presents no false damage identification, as shown in Fig. 5(b).

5. Sensor layout

When sensors are placed in a concentrated pattern, their geometry layout affects the superposition of wave packet excited by each transmitter, and thus it affects the energy focused in a given direction. Therefore, it is necessary to optimize sensor layout to form a concentrated beam and improve performance of damage identification. In order to investigate the directivity of sensor layout, the beamforming factors (*BF*) are introduced (Ostachowicz *et al.* 2009). For beam steering in isotropic medium, the wavefront excited by single sensor is circular. The *BF* describing the amplification in a given direction is defined as follows

$$BF(\theta) = \sum_{n=1}^{N} \exp\left[i\left(\vec{k}_\theta - \vec{k}_\phi\right)\vec{r}_n \right] \tag{11}$$

where k_θ is the wavenumber in the direction of interest; k_ϕ is the wavenumber in the focusing direction; and r is the location vector of the n-th sensor. The ideal *BF* should have slender main lobe and slight side lobes. During the excitation process, slender main lobe can concentrate energy in the focusing direction, while slight side lobes can alleviate energy leaking in the direction out of interest.

During the reception process, slender main lobe can concentrate high pixel at damage, while slight side lobes can alleviate false pixel assignment in other directions. When the energy leaked by side lobes is comparable to the energy of main lobe, these side lobes become grating lobes causing strong interference of damage identification.

In the next, the directivities of three relatively popular sensor layouts (see Fig. 7), i.e., the circular, spiral, and crossed patterns, were compared based on the *BF*. Holes with a diameter of 40 mm were drilled through the thickness of an 1 m × 1 m × 1 mm aluminum plate at the location of (142, -142) and (0, 350) mm, respectively. The time increment was set to 2×10^{-7} s, and the element was set to *S4R* in 1 × 1 mm. The *BF*s at 90° and 135° (where the actual damages locate) are presented in Fig. 8.

The beam steering in the focusing direction is processed through directional excitation and reception. For directional excitation, different transmitters are excited with calculated time delays to construct an intended wave superposition in the focusing direction and, accordingly, they amplify the potential damage reflection.
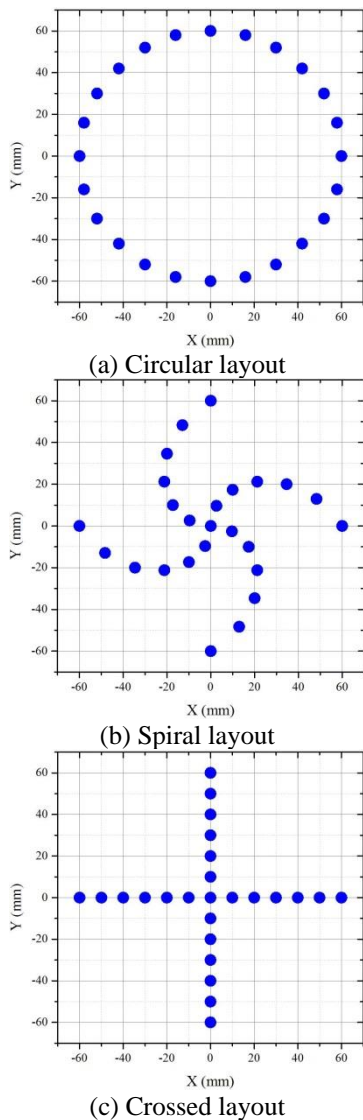
Since the distances from potential damage to each sensor are different, damage reflection reaches sensors at different time. To compensate these time differences, directional reception applies the same time delays on corresponding monitoring signals, making damage reflections appear at the same phase. With the directional excitation and reception, the sum of these shifted monitoring signals present an amplified wave peak of damage reflection. By multiplying the wave velocity with the time interval between excitation and the amplified damage reflection, the distance between potential damage and sensor array can be determined. Change of the time delays in directional excitation and reception can steer the beam (main lobe) to sweep in all directions. With a known azimuth and distance, damage images are reconstructed in a polar coordinate. In this case, the beam of propagating wave swept the plate with an increment of 1°. The main lobe, side lobes, and grating lobes (if exist) are marked, as shown in Fig. 9. Due to a non-biased geometry, the circular layout has the best capability of concentrating energy in the focusing direction (i.e., a slender main lobe) and depressing energy leaking in other directions (i.e., slight side lobes) among all the candidate layouts.
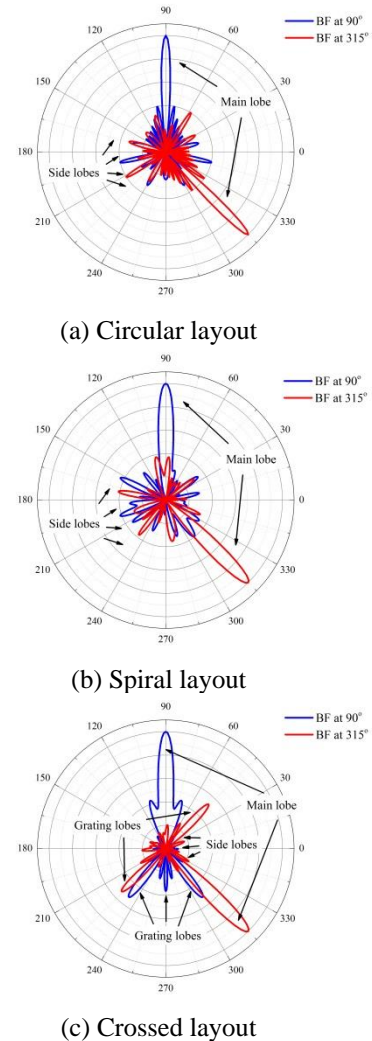

(a) Circular layout

(b) Spiral layout

(c) Crossed layout

Fig. 7 Different sensor arrays

(a) Circular layout

(b) Spiral layout

(c) Crossed layout

Fig. 8 Beamforming factors of different sensor arrays

(a) Circular layout

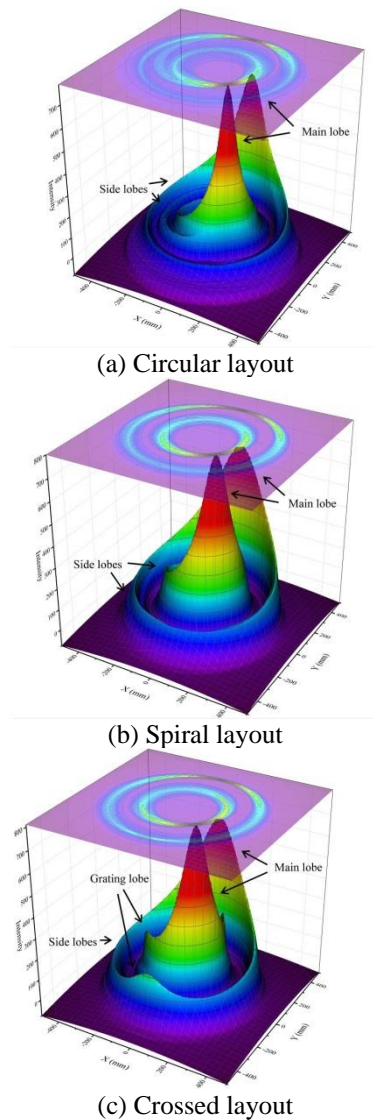

(b) Spiral layout

(c) Crossed layout

Fig. 9 Reconstructed damage images by different sensor arrays

Meanwhile, the crossed layout generates serious grating lobes. For the circular layout, the slender main lobe in Fig. 8(a) leads to a sharp damage peak in Fig. 9(a), while the slight side lobes lead to low interferences in other directions. For the spiral layout, the wide main lobe and high side lobes in Fig. 8(b) lead to a thick damage peak and large interferences in Fig. 9(b) as compared with the circular layout. For the crossed layout, the grating lobes at 45°, 225° and 270° in Fig. 8(c) lead to severe interferences in these directions, as shown in Fig. 9(c).

6. Conclusions

Lamb waves can travel inside the plate- or shell-type structure with little energy loss, thus providing suitable and effective damage identification for pipeline (Guan *et al.* 2017), ship (Sharma and Mukherjee 2015), and aircraft (Ihn and Chang 2008) structures. In this paper, wave velocity,

signal denoising, image reconstruction, and sensor layout essential to the Lamb wave-based damage identification are discussed in detail. A variety of principles, formulas, and instances associated with the four aspects above are presented, with the following conclusions being reached:

- Dispersion compensation and mode separation are desirable to obtain constant wave velocity and simple vibration mode. For damage identification in anisotropic media, directional wave velocity should be considered according to the path of wave propagation.
- Signal denoising can effectively improve the signal to noise ratio, and make damage-related wave features more distinctive in monitoring signals. The damage images produced by purified signals have higher quality than the ones produced by noisy signals.
- Different algorithms influence the reconstruction of damage images. The DAS algorithm owns higher resolution, while the RAPID enjoys higher robustness.
- By calculating beamforming factors, the directivity of sensor array can be quantitatively investigated. The sensor array with a slender main lobe and slight side lobes can accurately identify damage and depress interferences in other directions.

On the other hand, Lamb wave-based damage identification is still immature accompanied with the following interesting but challenging aspects as path forward:

- Development of sensor technology

The real-time damage identification requires repeatable Lamb wave excitation and reception by sensors implanted into structures. To this end, these sensors should have certain strength and compatible deformation to prevent sensor rupture and bring no compromise to structural performance. Moreover, these sensors should be durable during service life of structures, and/or they can be easily replaced once after failure. On the other hand, self-power and wireless reception (Padiyar and Balasubramaniam 2014) are promising topics for the application of Lamb waves.

- Realization of global identification

Lamb waves provide a local method to identify small damages in structures. However, optimal sensor layout is necessary for the extension of this local method to global damage identification (Salmanpour *et al.* 2017). The density of sensor should vary with the complexity of structural geometry to secure an efficient and accurate communication of sensor network. Dense sensors should cover complex geometry (Yu *et al.* 2017), e.g., structural boundary, stiffener, and hole; while sparse sensors should cover substantial areas with simple geometry (Wang *et al.* 2016). The combination of distributed sensors and directional array are expected to facilitate the global damage identification.

- Interpretation of monitoring signal

The mode conversion (Hennings and Lammering 2016) generates other types of elastic wave during Lamb wave excitation and scattering, introducing interferences in monitoring signals. In addition, environmental factors (Zou *et al.* 2015) influence the propagation of Lamb waves, causing monitoring signal changes unrelated to damages. Therefore, adaptive signal processing (Masurkar and Yelve 2017) and intelligent pattern recognition (Miller and

Hinders 2014) are expected to extract damage-related wave features and develop sensitive damage indices.

- Application of nonlinear wave

The damage, such as the zigzag geometry of cracks (Poddar and Giurgiutiu 2016), semi-contact at delamination in composites (Gauthier *et al.* 2017), and randomly distributed micro defects (Masserey and Fromme 2017) due to corrosion, fatigue and fire, exert non-linear influence to Lamb wave propagation. Therefore, nonlinear Lamb waves are fundamentally suitable to identify such types of damage (Zhao *et al.* 2017). The application of nonlinear Lamb waves is expected to improve the sensitivity to various damage which cannot be appropriately identified by linear Lamb waves (Minato and Ghose 2017).

Acknowledgements

References

Ambrozinski, L. and Stepinski, T. (2017), "Robust polarization filter for separation of Lamb wave modes acquired using a 3D laser vibrometer", *Mech. Syst. Signal Pr.*, **93**, 368-378.

Aryan, P., Kotousov, A., Ng, C.T. and Cazzolato, B.S. (2017), "A baseline-free and non-contact method for detection and imaging of structural damage using 3D laser vibrometry", *Struct. Control Health Monit.*, **24**(4), e1894.

Birgani, P.T., Sodagar, S. and Shishesaz, M. (2017), "Generation of low-attenuation Lamb wave modes in three-layer adhesive joints", *Int. J. Acoust. Vib.*, **22**(1), 51-57.

Bonnel, J., Caporale, S. and Thode, A. (2017), "Waveguide mode amplitude estimation using warping and phase compensation", *J. Acoust. Soc. Am.*, **141**(3), 2243-2255.

Cai, J., Shi, L., Yuan, S. and Shao, Z. (2011), "High spatial resolution imaging for structural health monitoring based on virtual time reversal", *Smart Mater. Struct.*, **20**(5).

Cai, J., Yuan, S.F. and Wang, T.G. (2017), "Signal construction-based dispersion compensation of Lamb waves considering signal waveform and amplitude spectrum preservation", *Materials*, **10**(1), 22.

Chen, J., Yuan, S.F., Qiu, L., Cai, J. and Yang, W.B. (2016), "Research on a Lamb wave and particle filter-based on-line crack propagation prognosis method", *Sensors*, **16**(3), 21.

De Marchi, L., Marzani, A., Moll, J., Kudela, P., Radzienski, M. and Ostachowicz, W. (2017), "A pulse coding and decoding strategy to perform Lamb wave inspections using simultaneously multiple actuators", *Mech. Syst. Signal Pr.*, **91**, 111-121.

Fan, W. and Qiao, P. (2011), "Vibration-based damage identification methods: a review and comparative study", *Struct. Health Monit.*, **10**(1), 83-111.

Farrar, C.R. and Worden, K. (2007), "An introduction to structural health monitoring, Philosophical Transactions of the Royal Society A: Mathematical", *Phys. Eng. Sci.*, **365**, 303-315.

Fei, Y., Roger, R. and Joseph, R. (2010), "Ultrasonic guided wave imaging techniques in structural health monitoring", *J. Intel. Mat. Syst. Str.*, **21**(3), 377-384.

Gauthier, C., El-Kettani, M., Galy, J., Predoi, M., Leduc, D. and Izbicki, J. (2017), "Lamb waves characterization of adhesion levels in aluminum/epoxy bi-layers with different cohesive and adhesive properties", *Int. J. Adhesion and Adhesives*, **74**, 15-20.

Guan, R., Lu, Y., Duan, W. and Wang, X. (2017), "Guided waves for damage identification in pipeline structures: A review", *Struct. Control Health Monit.*, **24**(11).

Hennings, B. and Lammering, R. (2016), "Material modeling for the simulation of quasi-continuous mode conversion during Lamb wave propagation in CFRP-layers", *Compos. Struct.*, **151**, 142-148.

Ihn, J.B. and Chang, F.K. (2008), "Pitch-catch active sensing methods in structural health monitoring for aircraft structures", *Struct. Health Monit.*, **7**(1), 5-19.

Kabir, M.A. and Shahnaz, C. (2012), "Denoising of ECG signals based on noise reduction algorithms in EMD and wavelet domains", *Biomed. Signal Process. Control*, **7**(5), 481-489.

Malinowski, P., Wandowski, T. and Ostachowicz, W. (2011), "Damage detection potential of a triangular piezoelectric configuration", *Mech. Syst. Signal Pr.*, **25**(7), 2722-2732.

Masserey, B. and Fromme, P. (2017), "Analysis of high frequency guided wave scattering at a fastener hole with a view to fatigue crack detection", *Ultrasonics*, **76**, 78-86.

Masurkar, F.A. and Yelve, N.P. (2017), "Optimizing location of damage within an enclosed area defined by an algorithm based on the Lamb wave response data", *Appl. Acoust.*, **120**, 98-110.

Miller, C.A. and Hinders, M.K. (2014), "Classification of flaw severity using pattern recognition for guided wave-based structural health monitoring", *Ultrasonics*, **54**(1), 247-258.

Minato, S. and Ghose, R. (2017), "Low-frequency guided waves in a fluid-filled borehole: simultaneous effects of generation and scattering due to multiple fractures", *J. Appl. Phys.*, **121** (10).

Mitra, M. and Gopalakrishnan, S. (2016), "Guided wave based structural health monitoring: A review", *Smart Mater. Struct.*, 25 (5).

Muller, A., Robertson, B., Gaydecki, P., Gresil, M. and Soutis, C. (2017), "Structural health monitoring using Lamb wave reflections and total focusing method for image reconstruction", *Appl. Compos. Mater.*, **24**(2), 553-573.

Ostachowicz, W., Kudela, P., Malinowski, P. and Wandowski, T. (2009), "Damage localisation in plate-like structures based on PZT sensors", *Mech. Syst. Signal Pr.*, **23**(6), 1805-1829.

Padiyar, J.M. and Balasubramaniam, K. (2014), "Lamb-wave-based structural health monitoring technique for inaccessible regions in complex composite structures", *Struct. Control Health Monit.*, **21**(5), 817-832.

Pant, S., Laliberte, J., Martinez, M. and Rocha, B. (2014), "Derivation and experimental validation of Lamb wave equations for an n-layered anisotropic composite laminate", *Compos. Struct.*, **111**, 566-579.

Poddar, B. and Giurgiutiu, V. (2016), "Scattering of Lamb waves from a discontinuity: an improved analytical approach", *Wave Motion*, **65**, 79-91.

Ratassepp, M., Fan, Z. and Lasn, K. (2016), "Wave mode extraction from multimodal wave signals in an orthotropic composite plate", *Ultrasonics*, **71**, 223-230.

Salmanpour, M.S., Khodaei, S. and Aliabadi, H. (2017), "Transducer placement optimisation scheme for a delay and sum damage detection algorithm", *Struct. Control Health Monit.*, **24**(4).

Sause, M.G.R., Hamstad, M.A. and Horn, S. (2013), "Finite element modeling of Lamb wave propagation in anisotropic hybrid materials", *Composites Part B: Eng.*, **53**, 249-257.

Sharma, S. and Mukherjee, A. (2015), "Ultrasonic guided waves for monitoring corrosion in submerged plates", *Struct. Control Health Monit.*, **22**(1), 19-35.

Su, Z., Ye, L. and Lu, Y. (2006), "Guided Lamb waves for identification of damage in composite structures: a review", *J. Sound Vib.*, **295**(3-5), 753-780.

Tao, C., Ji, H., Qiu, J., Zhang, C., Wang, Z. and Yao, W. (2017), "Characterization of fatigue damages in composite laminates using Lamb wave velocity and prediction of residual life", *Compos. Struct.*, **166**, 219-228.

Verona, E., Anisimkin, V.I., Osipenko, V.A. and Voronova, N.V. (2017), "Quasi longitudinal Lamb acoustic modes along ZnO/Si/ZnO structures", *Ultrasonics*, **76**, 227-233.

Wang, C.H., Rose, J.T. and Chang, F.K. (2004), "A synthetic time-reversal imaging method for structural health monitoring", *Smart Mater. Struct.*, **13**(2), 415-423.

Wang, L. and Yuan, F.G. (2007), "Group velocity and characteristic wave curves of Lamb waves in composites: modeling and experiments", *Compos. Sci. Technol.*, **67**(7-8), 1370-1384.

Wang, Q., Hong, M. and Su, Z. (2016), "A sparse sensor network topologized for cylindrical wave-based identification of damage in pipeline structures", *Smart Mater. Struct.*, **25**(7).

Wang, Z. and Qiao, P. (2017), "Backward wave separation method in a single transmitter and multi-receiver sensor array for improved damage identification of two-dimensional structures", *Int. J. Damage Mech.*, **26**(2), 229-250.

Wang, Z., Qiao, P. and Shi, B. (2016), "Application of soft-thresholding on the decomposed Lamb wave signals for damage detection of plate-like structures", *Measurement*, **88**, 417-427.

Yang, B., Xuan, F., Chen, S., Zhou, S., Gao, Y. and Xiao, B. (2017), "Damage localization and identification in WGF/epoxy composite laminates by using Lamb waves: experiment and simulation", *Compos. Struct.*, **165**, 138-147.

Yang, L. and Ume, I.C. (2017), "Measurement of weld penetration depths in thin structures using transmission coefficients of laser-generated Lamb waves and neural network", *Ultrasonics*, **78**, 96-109.

Yang, Y., Peng, Z., Zhang, W., Meng, G. and Lang, Z. (2016), "Dispersion analysis for broadband guided wave using generalized warblet transform", *J. Sound Vib.*, **367**, 22-36.

Yu, L. and Giurgiutiu, V. (2008), "In situ 2-D piezoelectric wafer active sensors arrays for guided wave damage detection", *Ultrasonics*, **48**(2), 117-134.

Yu, X., Ratassepp, M. and Fan, Z. (2017), "Damage detection in quasi-isotropic composite bends using ultrasonic feature guided waves", *Compos. Sci. Technol.*, **141**, 120-129.

Zeng, L., Lin, J. and Huang, L. (2017), "A modified Lamb wave time-reversal method for health monitoring of composite structures", *Sensors*, **17**(5).

Zeng, L., Lin, J., Bao, J., Joseph, P. and Huang, L. (2017), "Spatial resolution improvement for Lamb wave-based damage detection using frequency dependency compensation", *J. Sound Vib.*, **394**, 130-145.

Zhang, G., Gao, W., Song, G. and Song, Y. (2017), "An imaging algorithm for damage detection with dispersion compensation using piezoceramic induced lamb waves", *Smart Mater. Struct.*, **26**(2).

Zhao, Y., Li, F., Cao, P., Liu, Y., Zhang, J., Fu, S., Zhang, J. and Hu, N. (2017), "Generation mechanism of nonlinear ultrasonic Lamb waves in thin plates with randomly distributed micro-cracks", *Ultrasonics*, **79**, 60-67.

Zhu, K., Qiang, X. and Liu, B. (2017), "A reverberation-ray matrix method for guided wave-based non-destructive evaluation", *Ultrasonics*, **77**, 79-87.

Zou, D.J., Liu, T., Liang, C., Huang, Y., Zhang, F. and Du, C. (2015), "An experimental investigation on the health monitoring of concrete structures using piezoelectric transducers at various environmental temperatures", *J. Intel. Mat. Syst. Str.*, **26**(8), 1028-1034.

BS